The International Journal of Advanced Manufacturing Technology (2020) 106:2391–2402
https://doi.org/10.1007/s00170-019-04780-1

ORIGINAL ARTICLE

Mechanics and dynamics research considering the tool radial runout effect in plunge milling

Haining Gao[1] · Hongdan Shen[1] · Xianli Liu[2] · Rongyi Li[2]

Received: 29 July 2019 / Accepted: 2 December 2019 / Published online: 20 December 2019

Abstract
The tool radial runout effect in milling process has a significant impact on milling mechanics and dynamics, which increases the difficulty of accurate characterization of milling process. According to the cutter-workpiece contact relationship, the instantaneous chip thickness model considering the tool radial runout effect is established, and the prediction model of plunge milling force is obtained by combining the instant rigidity force model. The dynamical model with three degrees of freedom is established according to the characteristics of plunge milling and the time-varying delay effect caused by tool radial runout. The stability lobe diagram of the plunge milling process is obtained by the improved semi-discrete method. The simulation results are in good agreement with the experimental results, which verify the correctness of the model. The results show that the tool radial runout effect can improve the milling stability in a certain speed range. The effect of the tool radial runout on bifurcation frequency is also studied. It is found that the tool radial runout effect can produce period 1 bifurcation frequency in the milling non-stationary process and double the period 2 bifurcation and Hopf bifurcation frequency. The research results can provide theoretical support for accurate characterization and optimization of process parameters in plunge milling process.

Keywords The tool radial runout · Cutting force · Milling stability · Bifurcation frequency · Plunge milling

Nomenclature

R_1,R_2	The actual cutting radius of each tooth
ϕ_1,ϕ_2	The actual interdental angle of each tooth
ϕ_{st},ϕ_{ex}	The actual cut-in and cut-out angles of each tooth
K_a,K_r,K_t	Cutting coefficients in radial, feed, and tangential directions
F_a,F_r,F_t	Cutting force in radial, feed, and tangential directions
$g(\phi_{i,j})$	The window function
$\ddot{x}(t)$,$\ddot{y}(t)$,$\ddot{z}(t)$	The vibration acceleration in X,Y,Z directions
$\dot{x}(t)$,$\dot{y}(t)$,$\dot{z}(t)$	The vibration velocity in X,Y,Z directions
$x(t)$,$y(t)$,$z(t)$	The vibration displacement X,Y,Z directions
ζ_i,ω_{ni},k_i	The damping ratio, natural frequency and stiffness
$h_{ii,j}$	The direction force coefficient matrix of the cutting system
T_j	The delay term
f_{SP}	The spindle rotation frequency
f_{TP}	The tooth passing frequency
f_H	Hopf bifurcation frequency
f_{P1}	Period 1 bifurcation frequency
f_{PD}	Period 2 bifurcation frequency
u	the characteristic multiplier
λ	The eigenvalue of the cutting system
T	The cutting vibration period
ρ	The eccentricity of cutter
θ_0	The eccentricity angle of cutter

1 Introduction

Plunge milling is a new type of processing developed in recent years. It is widely used in aerospace, hydropower and mold manufacturing industries due to its high processing efficiency. The length-diameter ratios of the required tool shank up to 14.9:1 in the plunge milling. When the runner of the Pelton turbine is roughed, it is easy to chatter, which accelerates tool

✉ Haining Gao
hngao@hrbust.edu.cn

[1] HuangHuai University, Zhumadian 463000, China

[2] Harbin University of Science and Technology, Harbin 150080, China

wear and tear, reduces surface quality, and severely restricts processing cost. Because of the errors of tool manufacturing and installation, the tool radial runout effect is easily caused in the machining process, which resulting in uneven force on each tooth and affects the milling mechanics and dynamics. How to effectively reveal the influence mechanism of the tool radial runout on cutting force and stability in plunge milling process has become a key problem to be solved urgently.

Cutting force is the basis for studying the cutting vibration, stability [1], the optimization of tool path [2], machining quality, and dimensional accuracy of the machining process. Therefore, the cutting force modeling has been widely investigated by scholars all over the world. Cutting force modeling methods are mainly divided into empirical method [3], analytical method [4], finite element method [5], and mechanical method [6]. The instant rigidity force model is used most extensively in cutting force modeling method. The cutting force in this model is assumed to be proportional to the instantaneous chip thickness. Therefore, the establishment of an instantaneous chip thickness model considering the tool radial runout becomes the key to predict the cutting force. Sutherland et al. [7] and Wang et al. [8] developed an iterative algorithm to calculate the chip thickness model considering the tool radial runout. Because the tool radial runout mainly affects the radial position of the cutter teeth, Kline et al. [9] developed a simplified model based on the different feed of each tooth. Wang et al. [10] proposed a cutting force prediction model considering the influence of the tool radial runout and tool vibration. Sun et al. [11] established an undeformed chip thickness model considering runout effect when the direction of tool axis changed continuously by using the sweep path of tool edge. Zhu et al. [12] proposed a moving edge element method to calculate the instantaneous undeformed chip thickness considering the tool radial runout. Zhou et al. [13] proposed a cutting force analysis model considering edge radius, material hardening effect, the tool radial runout, and variable sliding friction coefficient in micro-end milling cutter. Li et al. [14] proposed a general instantaneous undeformed chip thickness model considering the tool radial runout.

The time-frequency domain method is often used to solve the delay differential equation to obtain the critical machining parameters and then to form the stability lobe diagram of the milling process. The machining area is divided into the stable cutting zone and the unstable cutting zone, and then, the machining parameters can be reasonably selected from the stable cutting zone and finally the purpose of the stable cutting process is achieved [15]. The time-frequency domain method includes frequency domain method, discrete method, and numerical method [16]. The frequency domain method includes zero-order frequency domain method [17] and multi-frequency method [18]. Discrete method includes semi-discrete method [19], full discrete method [20], and time finite element method [21]. It is worth noting that the above work is performed under the assumption that there is only one delay term. It is generally assumed that the delay term is a constant whose value is the passage period of cutter tooth. Due to the influence of tool radial runout, the occurrence of state-dependent delay directly results in multiple delay items in milling. Insperger et al. [22] studied the influence of the tool radial runout on milling stability and frequency characteristics. The results show that the tool radial runout has no effect on stability, but has a significant impact on frequency characteristics. However, their research is still carried out under the assumption that the delay can be approximated to the passage period of the cutter teeth. Wan et al. [23] proposed an improved semi-discretization method to study the effects of multiple time delays caused by tool runout on milling stability. However, this method does not consider the periodic variation of time delay. Zhang et al. [24] proposed a new variable step-size numerical integration method to study the effect of tool radial runout on stable boundary. Zhang et al. [25] proposed a milling stability prediction method based on time-varying delay and tool runout effect. Subsequently, the influence of different the tool radial runout values on the milling dynamics is further analyzed [26].

It can be seen from the above literature that the tool radial runout has a great influence on milling mechanics and dynamics. The existing research literatures on tool radial runout mainly focus on end milling and ball end milling, but hardly involve the plunge milling process. The influence of tool radial runout on cutting force and stability in plunge milling process has not been effectively revealed. According to the action law of tool radial runout on the cutter-workpiece contact area in the plunge milling process, the instantaneous chip thickness model is established, and then, the cutting force prediction model is obtained. The dynamical model with three degrees of freedom is established according to the characteristics of plunge milling and the time-varying delay effect caused by tool radial runout. The stability lobe diagram of the plunge milling process is obtained by the improved semi-discrete method. The effect of the tool radial runout on bifurcation frequency is also studied. The research results can provide theoretical support for accurate characterization and optimization of process parameters in plunge milling process.

2 Plunge milling force modeling

The tool radial runout makes the cutting forces of different cutting edges on the same cutter teeth different, which seriously affects the service life of the cutter, the accuracy of the

workpiece, and the processing efficiency. Therefore, it must be controlled in the machining process. The cutting force modeling considering the tool radial runout is the key to achieve control. The cutting force model considering tool radial runout is shown in Fig. 1.

The actual cutting radius of each tooth is as follows.

$$\begin{cases} R_1 = \sqrt{R^2 + \rho^2 - 2R\rho\cos(\pi - \theta_0)} \\ R_2 = \sqrt{R^2 + \rho^2 - 2R\rho\cos(\theta_0)} \end{cases} \tag{1}$$

The actual interdental angles are as follows.

$$\begin{cases} \phi_1 = 2\pi - \phi_2 \\ \phi_2 = \arccos\left(\dfrac{R_1^2 + R_2^2 - (2R)^2}{2 \cdot R_1 \cdot R_2}\right) \end{cases} \tag{2}$$

The actual cut-in and cut-out angles of each tooth are as follows.

$$\begin{cases} \phi_{1st} = \dfrac{\pi}{2} + \arcsin\left(\dfrac{R - a_e}{R_1}\right) \\ \phi_{1ex} = \dfrac{\pi}{2} + \arccos\left(\dfrac{R_1^2 + (2a_c)^2 - R_1^2}{2 \cdot R_1 \cdot 2a_c}\right) \end{cases} \tag{3}$$

$$\begin{cases} \phi_{2st} = \dfrac{\pi}{2} + \arcsin\left(\dfrac{R - a_e}{R_2}\right) \\ \phi_{2ex} = \dfrac{\pi}{2} + \arccos\left(\dfrac{R_1^2 + (a_c)^2 - R_2^2}{2 \cdot R_1 \cdot a_c}\right) \end{cases} \tag{4}$$

The actual distance of each tooth moving in the feed direction is as follows.

$$\begin{cases} a_{c1}' = a_c + \sqrt{R_1^2 - (R - a_e)^2} - \sqrt{R_2^2 - (R - a_e)^2} \\ a_{c2}' = a_c + \sqrt{R_2^2 - (R - a_e)^2} - \sqrt{R_1^2 - (R - a_e)^2} \end{cases} \tag{5}$$

The instantaneous chip thickness of each tooth is calculated as follows.

$$h(\phi_{i,j}) = a_{cp}' \sin(\phi_{i,j}) p = 1, 2 \tag{6}$$

According to the instant rigidity force model proposed by Lee et al. [6], the tangential, radial, and axial cutting forces are obtained. The specific equations are as follows.

$$\begin{cases} F_t = K_{tc} \cdot h(\phi_{i,j}) \cdot f_z + K_{te} \cdot f_z \\ F_r = K_{rc} \cdot h(\phi_{i,j}) \cdot f_z + K_{re} \cdot f_z \\ F_a = K_{ac} \cdot h(\phi_{i,j}) \cdot f_z + K_{ae} \cdot f_z \end{cases} \tag{7}$$

The tangential, radial, and axial cutting forces are transformed into X, Y, and Z directions.

$$\begin{cases} F_x = \sum_1^N g(\phi_{i,j}) \left(-F_t \cos(\phi_{i,j}) - F_r \sin(\phi_{i,j})\right) \\ F_y = \sum_1^N g(\phi_{i,j}) \left(+F_t \sin(\phi_{i,j}) - F_r \cos(\phi_{i,j})\right) \\ F_z = \sum_1^N g(\phi_{i,j}) F_a \end{cases} \tag{8}$$

where $g(\phi_{i,j})$ is the window function, which is used to determine whether the tool is involved in cutting.

3 Stability analysis

According to the characteristics of axial feed in the process of plunge milling, the cutting system composed of spindle and tool is regarded as flexible body and the workpiece is regarded as rigid body. Therefore, the plunge milling system is simplified to a three-degree-of-freedom spring-damping system in the coordinate system, as shown in Fig. 2. The mathematical differential equation of the dynamic model of the plunge milling system is shown in Eq. (9).

$$\begin{pmatrix} \ddot{x}(t) \\ \ddot{y}(t) \\ \ddot{z}(t) \end{pmatrix} + \begin{pmatrix} 2\xi_x\omega_{nx} & 0 & 0 \\ 0 & 2\xi_y\omega_{ny} & 0 \\ 0 & 0 & 2\xi_z\omega_{nz} \end{pmatrix} \begin{pmatrix} \dot{x}(t) \\ \dot{y}(t) \\ \dot{z}(t) \end{pmatrix} + \begin{pmatrix} \omega_{nx}^2 & 0 & 0 \\ 0 & \omega_{ny}^2 & 0 \\ 0 & 0 & \omega_{nz}^2 \end{pmatrix} \begin{pmatrix} x(t) \\ y(t) \\ z(t) \end{pmatrix} =$$
$$\sum_{j=1}^{N} \left(R - \frac{R - a_e}{\sin\phi_{i,j}(t)}\right) \begin{pmatrix} \frac{\omega_{nx}^2}{k_x} & 0 & 0 \\ 0 & \frac{\omega_{ny}^2}{k_y} & 0 \\ 0 & 0 & \frac{\omega_{nz}^2}{k_z} \end{pmatrix} \begin{pmatrix} h_{xx}(t) & h_{xy}(t) & h_{xz}(t) \\ h_{yx}(t) & h_{yy}(t) & h_{yx}(t) \\ h_{zx}(t) & h_{zy}(t) & h_{zz}(t) \end{pmatrix} \begin{pmatrix} x(t) - x(t - T_j) \\ y(t) - y(t - T_j) \\ z(t) - z(t - T_j) \end{pmatrix} \tag{9}$$

$\ddot{x}(t), \ddot{y}(t), \ddot{z}(t), \dot{x}(t), \dot{y}(t), \dot{z}(t), x(t), y(t), z(t)$ are vibration acceleration, vibration velocity, and vibration displacement of cutting system in three directions, respectively. $\zeta_i, \omega_{ni}, k_i$ are damping ratio, natural frequency, and stiffness of the cutting system in

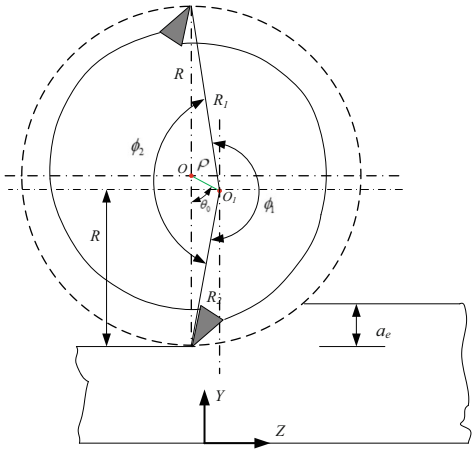

(a) The geometry of the tool runout

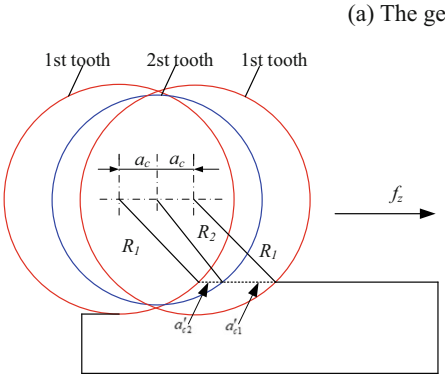

(b) Instantaneous chip thickness

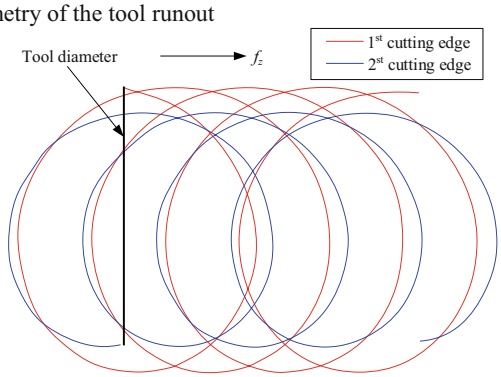

(c) Trochoidal trajectory of tool tip of the two teeth

Fig. 1 Plunge milling force model considering tool radial runout

three directions, respectively. $h_{ii,j}$is the direction force coefficient matrix of the cutting system. T_j is a delay term, $T_1 = (\phi_1 \cdot T)/360$, $T_2 = (\phi_2 \cdot T)/360$.

$$\begin{cases} h_{xx}(t) = \sum_{j=1}^{N} -g(\phi_j(t))\sin(\phi_j(t))\left[K_{tc}\cos(\phi_j(t)) + K_{rc}\sin(\phi_j(t))\right]\tan\psi \\ h_{xy}(t) = \sum_{j=1}^{N} -g(\phi_j(t))\cos(\phi_j(t))\left[K_{tc}\cos(\phi_j(t)) + K_{rc}\sin(\phi_j(t))\right]\tan\psi \\ h_{xz}(t) = \sum_{j=1}^{N} -g(\phi_j(t))\left[K_{tc}\cos(\phi_j(t)) + K_{rc}\sin(\phi_j(t))\right] \\ h_{yx}(t) = \sum_{j=1}^{N} g\left(\varphi_j(t)\right)\sin(\phi_j(t))\left[K_{tc}\sin(\phi_j(t)) - K_{rc}\cos(\phi_j(t))\right]\tan\psi \\ h_{yy}(t) = \sum_{j=1}^{N} g(\phi_j(t))\cos(\phi_j(t))\left[K_{tc}\sin(\phi_j(t)) - K_{rc}\cos(\phi_j(t))\right]\tan\psi \\ h_{yz}(t) = \sum_{j=1}^{N} g(\phi_j(t))\left[K_{tc}\sin(\phi_j(t)) - K_{rc}\cos(\phi_j(t))\right] \\ h_{zx}(t) = \sum_{j=1}^{N} g(\phi_j(t))\sin(\phi_j(t))K_{ac}\tan\psi \\ h_{zy}(t) = \sum_{j=1}^{N} g(\phi_j(t))\cos(\phi_j(t))K_{ac}\tan\psi \\ h_{zz}(t) = \sum_{j=1}^{N} g(\phi_j(t))K_{ac} \end{cases} \tag{10}$$

Using the Cauchy transform, Eq. (9) can be written in the following form:

$$u'(t) = A_i u(t) + \omega_a B_i u_{i-m+1} + \omega_b B u_{i-m} \tag{11}$$

Where

$$A_i = \begin{bmatrix} [0] & [I] \\ a_e[M]^{-1}[A(t)] - [\omega_n^2] & -[2\zeta\omega_n] \end{bmatrix}$$

$$B_i = \begin{bmatrix} [0] & [0] \\ \delta[M]^{-1}[A(t)] & [0] \end{bmatrix}$$

$$u(t) = \{x(t), y(t), z(t), \dot{x}(t), \dot{y}(t), \dot{z}(t)\}^T$$

$$u_i = u(t_i) = \{x(t), y(t), z(t), \dot{x}(t), \dot{y}(t), \dot{z}(t)\}^T$$

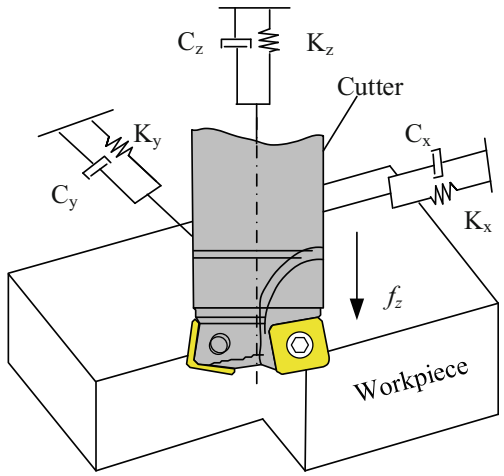

Fig. 2 3-DOF milling dynamics model

Table 1 The chemical composition of the workpiece material

Element	C	Si	Mn	S	P	Cr	Ni	Mo	N
Content (%)	≤0.05	≤0.70	≤1.00	≤0.010	≤0.030	15.0~16.5	4.5~5.5	0.8~1.20	≤0.05

$$\omega_a = \omega_b = \frac{1}{2}$$

Equation (10) is solved within a given time interval $t \in (t_i, t_{i+1})$ by the initial conditionu_i.

$$u_{j+1} = P_i u_i + \omega_a R_i u_{i-m+1} + \omega_b R_i u_{i-m} \tag{12}$$

where $P_i = \exp(A_i \Delta t), R_i = (\exp(A_i \Delta t) - I) A_i^{-1} B_i$.

The recurrence formula can be obtained from Eq. (12).

$$z_{i+1} = D_i z_i \tag{13}$$

where (3 m + 6) dimensional state vector can be expressed as follows.

$$z_i = col\left(x_i\ y_i\ z_i\ x_i^{'}\ y_i^{'}\ z_i^{'}\ x_{i-1}\ y_{i-1}\ z_{i-1} \cdots x_{i-m}\ y_{i-m}\ z_{i-m}\right) \tag{14}$$

The coefficient matrix$D_i$can be expressed as follows

$$D_t = \begin{bmatrix}
P_{i,11} & P_{i,12} & \cdots & P_{i,19} & 0 & \cdots & 0 & \omega_a R_{i,11} & \omega_a R_{i,12} & \omega_a R_{i,13} & \omega_b R_{i,11} & \omega_a R_{i,12} & \omega_a R_{i,13} \\
P_{i,21} & P_{i,22} & \cdots & P_{i,29} & 0 & \cdots & 0 & \omega_a R_{i,21} & \omega_a R_{i,22} & \omega_a R_{i,23} & \omega_b R_{i,21} & \omega_b R_{i,22} & \omega_b R_{i,23} \\
\vdots & \vdots & \ddots & \vdots & \vdots & \ddots & \vdots & \vdots & \vdots & \vdots & \vdots & \vdots & \vdots \\
P_{i,91} & P_{i,92} & \cdots & P_{i,99} & 0 & \cdots & 0 & \omega_a R_{i,91} & \omega_a R_{i,92} & \omega_a R_{i,93} & \omega_b R_{i,91} & \omega_b R_{i,91} & \omega_b R_{i,93} \\
1 & 0 & 0 & 0 & 0 & \cdots & 0 & 0 & 0 & 0 & 0 & 0 & 0 \\
0 & 1 & 0 & 0 & 0 & \cdots & 0 & 0 & 0 & 0 & 0 & 0 & 0 \\
0 & 0 & \ddots & 0 & 0 & \cdots & 0 & 0 & 0 & 0 & 0 & 0 & 0 \\
0 & 0 & 0 & 0 & 1 & \cdots & 0 & 0 & 0 & 0 & 0 & 0 & 0 \\
\vdots & \vdots & \vdots & \vdots & \vdots & \ddots & \vdots & \vdots & \vdots & \vdots & \vdots & \vdots & \vdots \\
0 & 0 & 0 & 0 & 0 & \cdots & 1 & 0 & 0 & 0 & 0 & 0 & 0 \\
0 & 0 & 0 & 0 & 0 & \cdots & 0 & 1 & 0 & 0 & 0 & 0 & 0 \\
0 & 0 & 0 & 0 & 0 & \cdots & 0 & 0 & 1 & 0 & 0 & 0 & 0 \\
0 & 0 & 0 & 0 & 0 & \cdots & 0 & 0 & 0 & 1 & 0 & 0 & 0
\end{bmatrix}$$

According to the Floquet theory [27], if the characteristic value is greater than 1, the milling system is unstable. If the modulus of the characteristic value is equal to 1, the critical stability of the milling system. If the characteristic values are less than 1, the system is stable.

4 Vibration frequency

The common vibration forms are forced vibration and self-excited vibration, all of which have their corresponding vibration frequencies. For forced vibration, its vibration frequency is mainly the spindle rotation frequency and the tooth passing frequency.

The spindle rotation frequency can be denoted byf_{SP}.

$$f_{SP} = \frac{2\pi kn}{60}[rad/s] = \frac{kn}{60}[Hz],\ k = 0, 1, 2\ldots \tag{15}$$

The tooth passing frequency can be denoted byf_{TP}.

$$f_{TP} = \frac{2\pi knN}{60}[rad/s] = \frac{knN}{60}[Hz],\ k = 0, 1, 2\ldots \tag{16}$$

Whether stable cutting or unstable cutting, there will be the spindle rotation frequency and the tooth passing frequency in the plunge milling. In addition to the above two frequencies, there are also different bifurcation frequencies in the unstable cutting. The bifurcation frequency can be subdivided into Hopf bifurcation, period 1 bifurcation and period 2 bifurcation. The common bifurcations are Hopf bifurcation and period 2 bifurcation [22]. The stability of the system can be determined by the relative magnitude between the modulus of the characteristic multiplier and 1 in Floquet theory. (1) Hopf bifurcation: the characteristic multiplier passes through the unit circle in conjugate complex form. The corresponding bifurcation frequency is

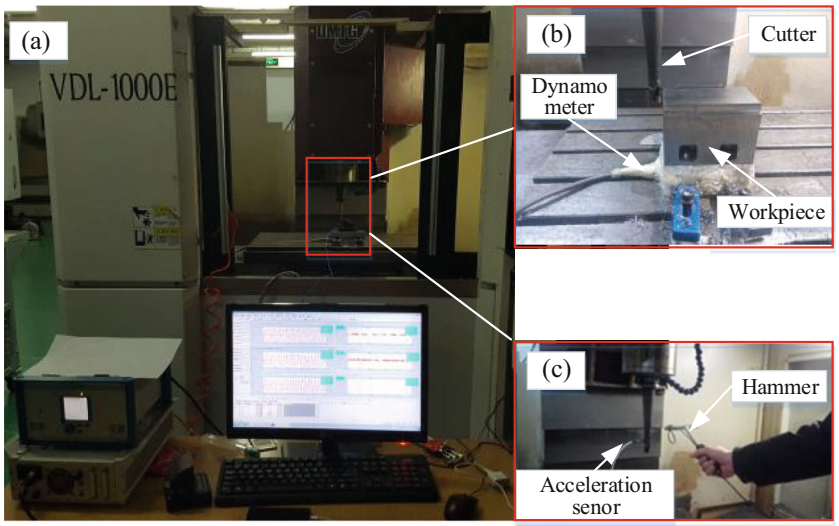

Fig. 3 The plunge milling processing setup. **a** The experimental site. **b** Local enlarged drawing of plunge milling. **c** Modal experiment

$$f_H = \pm\frac{\mathrm{Im}(\ln(u))}{T} + \frac{2\pi k}{T}[rad/s] = \pm\frac{\mathrm{Im}(\ln(u))}{2\pi T} + \frac{2\pi k}{2\pi T}[Hz], k = 0, 1, 2\ldots \quad (17)$$

(2) Period 1 bifurcation: the characteristic multiplier passes through the unit circle on the positive real axis. The corresponding bifurcation frequency is

$$f_{P1} = \frac{2\pi k}{T}[rad/s] = \frac{k}{T}[Hz], k = 0, 1, 2\ldots \quad (18)$$

(3) Period 2 bifurcation: the characteristic multiplier passes through the unit circle on the negative real axis. The corresponding bifurcation frequency is

$$f_{PD} = \frac{\pi}{T} + \frac{2\pi k}{T}[rad/s] = \frac{1}{2T} + \frac{k}{T}[Hz], k = 0, 1, 2\ldots \quad (19)$$

According to the vibration theory, the characteristic multiplier formula is as follows.

$$u = e^{(\lambda T)} \quad (20)$$

where $T$is the cutting vibration period and λ is the eigenvalue of the cutting system.

Table 2 Modal parameters of the plunge milling system

Direction	Order	Natural frequency (Hz)	Damping	Rigidity (N/m)
X	1	723	0.0435	1.74×10^7
	2	1600	0.0179	3.2×10^7
Y	1	663	0.0485	1.71×10^7
	2	1600	0.0183	3.18×10^7
Z	1	553	0.0413	3.01×10^7
	2	1104	0.0165	4.3×10^7

5 Experiment

5.1 Experiment setup

The Dalian machine tool vertical machining center VDL-1000E was employed in this experiment. The Seco plunge milling tool (R217.79-1020.RE-09-2AN) with a radius of 10 mm was used in this experiment. The workpiece material is 0Cr13Ni4Mo. After heat treatment, the hardness of workpiece is 293HBW. The chemical composition of the workpiece material is shown in Table 1. The plunge milling force was measured by three-direction piezoelectric dynamometer. The model of the experimental dynamometer is Kistler9257B. The conduction sensitivity of the selected PCB sensor is 10.42 mv/g. The charge amplifier model used in the experiment is Kistler5007 and the Donghua DH5922 signal acquisition system is used for data acquisition and analysis. The plunge milling processing setup is shown in Fig. 3. The force hammer with a sensitivity of 3.41 pC/N was used for the modal test to obtain the intrinsic parameters of workpiece and cutting system, as shown in Table 2. The cutting parameters used to verify the model are shown in Table 3.

Table 3 Cutting parameters

NO.	n (rpm)	a_e (mm)	f_z (mm/tooth)	a_p (mm)
1	1500	0.5	0.07	10
2	1500	0.7	0.08	
3	1500	1.0	0.09	
4	2000	0.5	0.08	
5	2000	0.7	0.09	
6	2000	1.0	0.07	
7	2500	0.5	0.09	
8	2500	0.7	0.07	
9	2500	1.0	0.08	

Table 4 The force coefficient of plunge milling force

K_{tc} (N/mm^2)	K_{te} (N/mm)	K_{rc} (N/mm^2)	K_{re} (N/mm)	K_{ac} (N/mm^2)	K_{ae} (N/mm)
3848.4	20.4	1960.9	22.1	2550.4	8.5

5.2 Cutting force coefficient

The methods for calculating the cutting force coefficients can be divided into the average cutting force method and the instantaneous cutting force method. The cutting force coefficient is affected by the cutting parameters [28] and the dynamic characteristics of the machining system [29], which is not considered in this paper. The average cutting force method is used to calculate the cutting force coefficients of the plunge milling process in this paper. The results are shown in Table 4. The specific solution process is detailed in Ref. [30].

5.3 Identification of the tool radial runout parameters

Accurate identification of the tool radial runout parameters is the premise of cutting force and stability prediction. ARMAREGO et al. [31] proposed an iterative optimal fitting method for estimating the tool radial runout from the measured value of milling force. LIANG et al. [32] used convolution integral to obtain the frequency domain model of milling force and established the explicit function of the tool radial runout with the Fourier series coefficient of the spindle frequency milling force component as the variable. WANG et al. [33] proposed a method for identifying the tool radial runout based on the spindle frequency milling force component, which does not need to know the milling force coefficient value in advance. All the above methods need to decompose the milling force in frequency domain. Based on the identification method of the cutter radial runout parameters proposed by Wan et al. [34], the

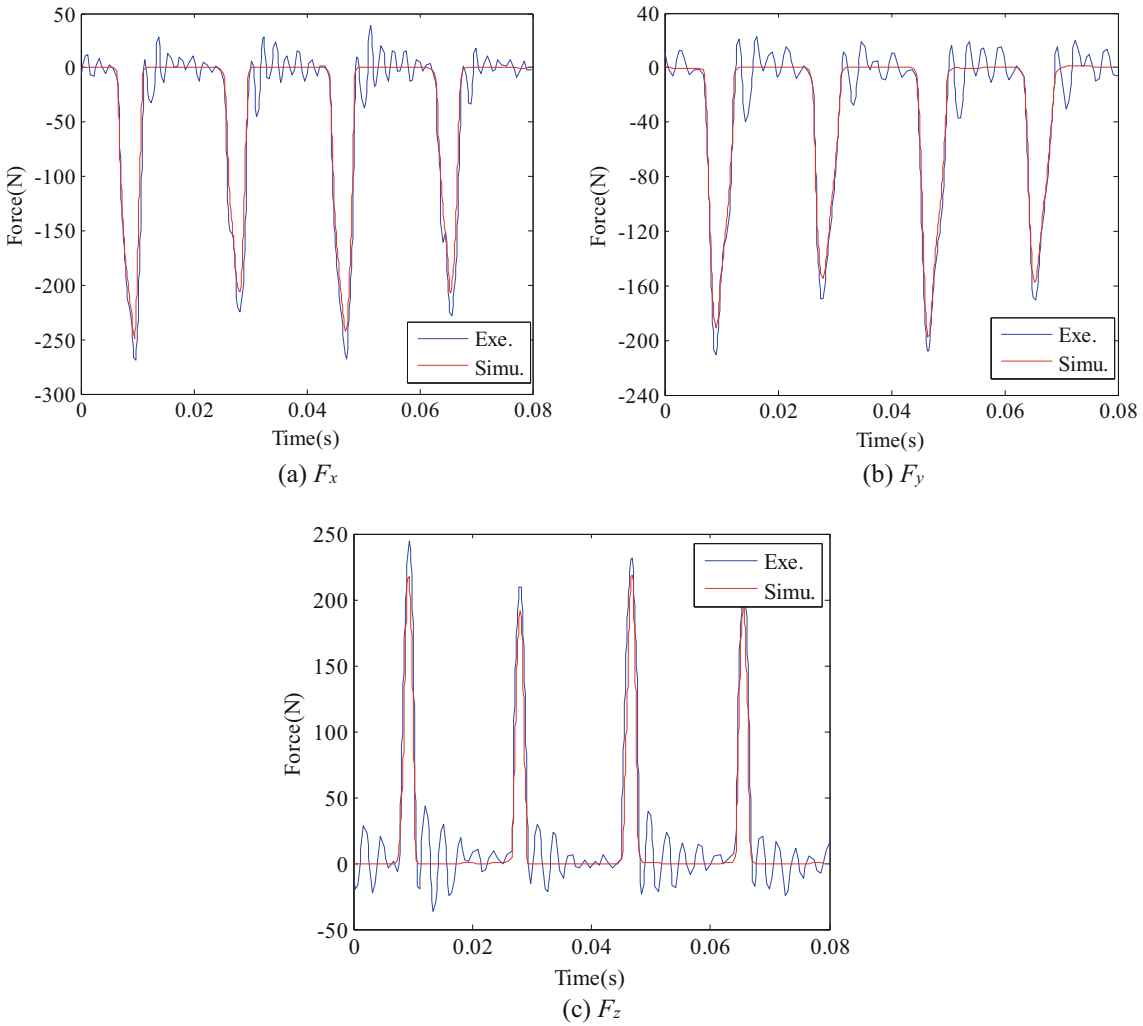

Fig. 4 Simulation and experimental results of cutting force, Exe.-experimental, Simu.-simulation

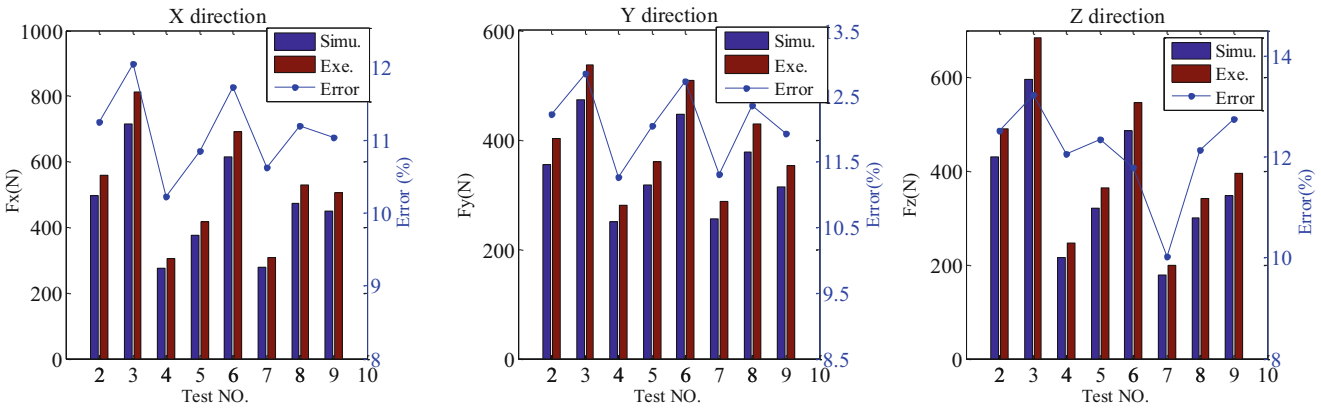

Fig. 5 Simulation and experimental results of cutting force, Exe.-experimental, Simu.-simulation

cutter radial runout parameters in plunge milling process are obtained as follows. $\rho = 10.4\mu m, \theta_0 = 23.1°$.

6 Results

6.1 The cutting force

The simulation and experimental force comparison results with test 1 in the X, Y, and Z directions are shown in Fig. 4.

It is found that the simulation forces in X, Y and Z directions are in good agreement with the experimental forces. The maximum errors are 10.71%, 11.43%, and 12.19%, respectively. The comparison results of the maximum simulation force and the experimental force and the maximum simulation error with tests 2–9 are shown in Fig. 5. The maximum errors in X, Y, and Z directions are 12.04%, 12.84%, and 13.23%, respectively. The errors are within acceptable range, which confirm the correctness of the cutting force model. Meanwhile, it is found that the maximum difference of cutting forces of different cutting edges on the same cutter in the X, Y, and Z directions caused by the radial runout of the tool is 16%, 18.42%, and 18.18%, respectively.

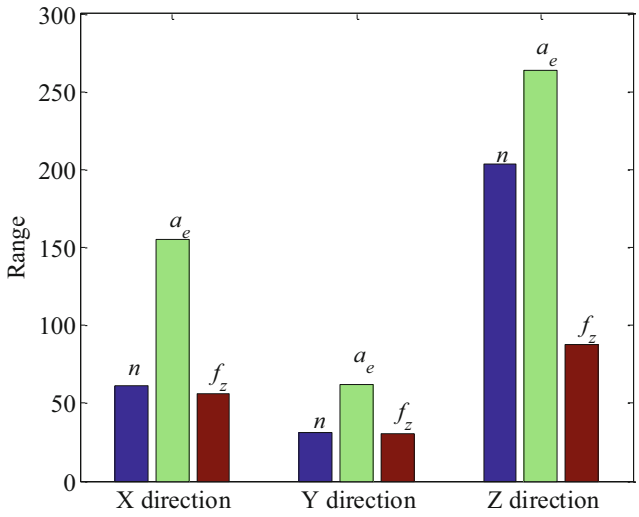

Fig. 6 The range

Based on the cutting force obtained under the parameters in Table 2, combined with the range analysis method, the range of each factor is shown in Fig. 6.

It can be seen from Fig. 6 that the radial cutting width has the greatest influence on the plunge milling force, followed by the spindle speed, and finally the feed per tooth.

6.2 Milling stability

The stability lobe diagrams with and without considering the tool radial runout effect are shown in Fig. 7. A series of experiments were carried out to verify the validity of the predicted stable lobe diagram. Specific experimental cutting parameters and machining state are given in Table 5 ($a_p = 10$ mm, $fz = 0.07$ mm/tooth).

Two points A and B are selected for experimental verification in order to verify the correctness of the predicted results. Figure 7b and c are acceleration signals in time domain. Figure 7d and e are Fourier transform results of acceleration signals.

The maximum amplitude of acceleration signal in point A is 4 m/s2, and its amplitude variation has better convergence, as shown in Fig. 7b. Fourier transform is applied to the acceleration signal in time domain, and the result is shown in Fig. 7d. It is found that the spectrum energy mainly concentrates on the cutter teeth passing frequency and its higher harmonics. The maximum amplitude of acceleration signal in point B is 22 m/s2, and its amplitude variation law is from small to large, which does not have convergence, as shown in Fig. 7c. Fourier transform is applied to the acceleration signal in time domain, and the result is shown in Fig. 7e. It is found that the spectrum energy is mainly concentrated near the first-order natural frequency of the plunge milling system. In conclusion, A is the cutting stability point and B is the cutting chatter point.

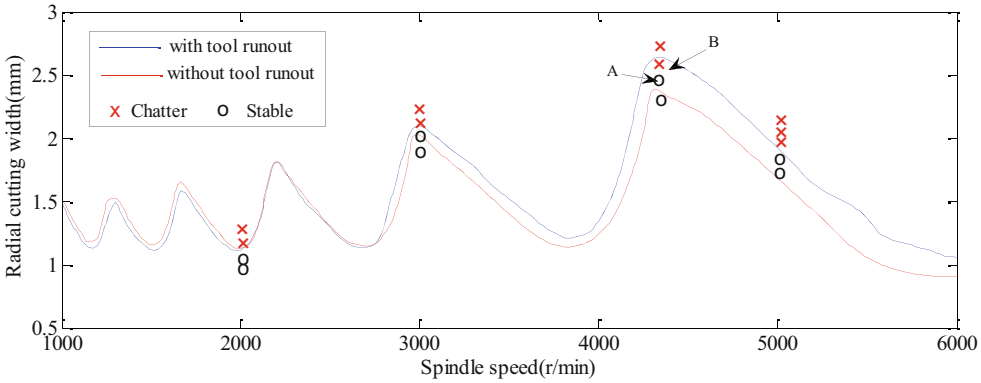

(a) The stability lobe diagram

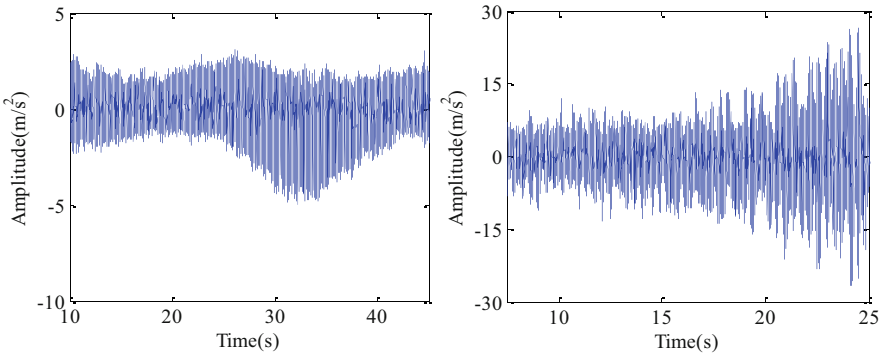

(b) Displacement Vibration Signal (PointA) (c) Displacement Vibration Signal (PointB)

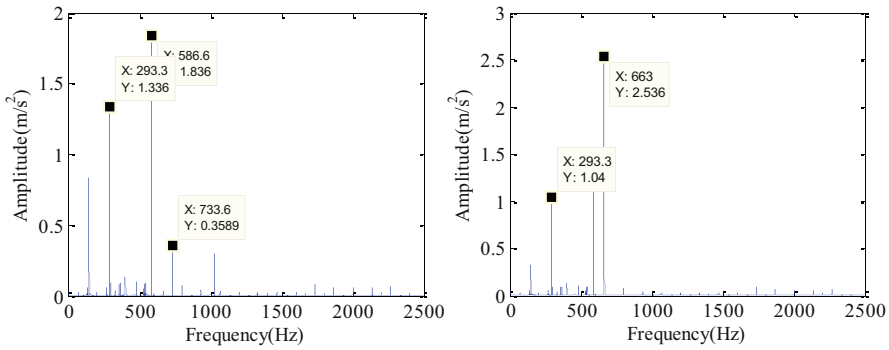

(d) Spectrum Analysis (Point A) (e) Spectrum Analysis (Point B)

Fig. 7 Experimental verification of milling stability. **a** The stability lobe diagram. **b** Displacement vibration signal (point A). **c** Displacement vibration signal (point B). **d** Spectrum analysis (point A). **e** Spectrum analysis (point B)

Table 5 Machining state with different conditions

	Cutting Parameters		Machining state		Cutting parameters		Machining state
No.	n (rpm)	a_e (mm)		No.	n (rpm)	a_e (mm)	
1	2000	0.95	Stable	10(A)	4400	2.42	Stable
2	2000	1.05	Stable	11(B)	4400	2.52	Chatter
3	2000	1.15	Chatter	12	4400	1.65	Chatter
4	2000	1.25	Chatter	13	5000	1.75	Stable
5	3000	1.92	Stable	14	5000	1.85	Stable
6	3000	2.02	Stable	15	5000	1.95	Stable
7	3000	2.12	Chatter	16	5000	2.05	Chatter
8	3000	2.22	Chatter	17	5000	2.15	Chatter
9	4400	2.32	Stable				

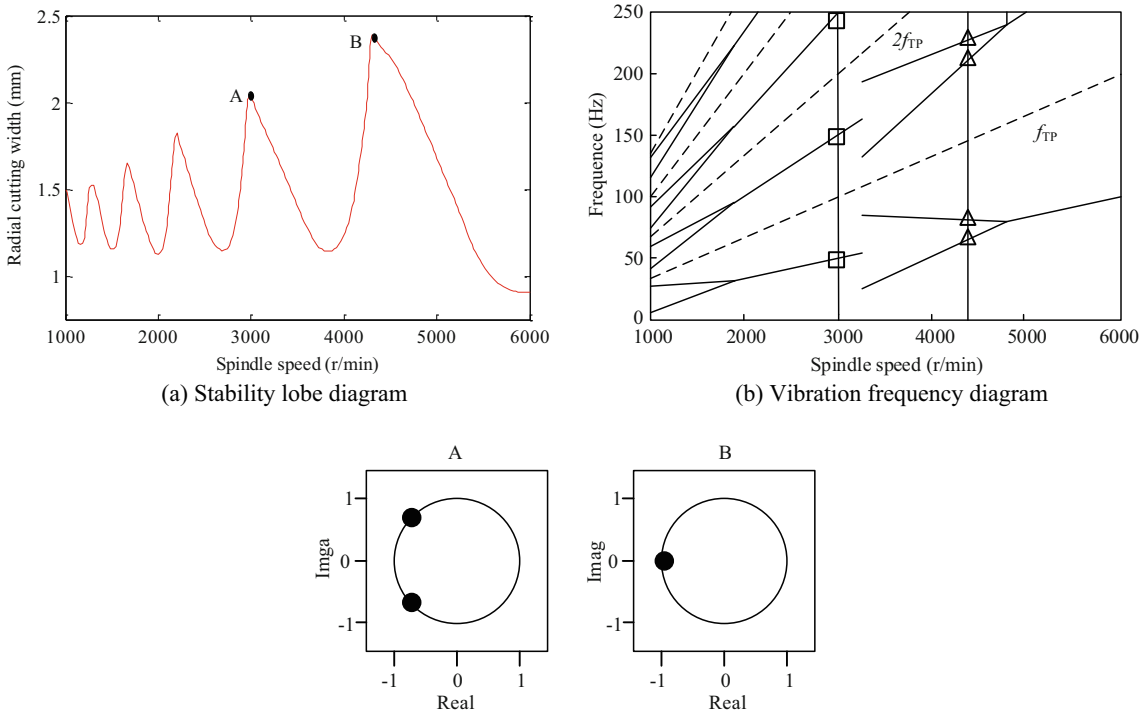

(a) Stability lobe diagram (b) Vibration frequency diagram

(c) The relationship between characteristic multiplier and unit circle

Fig. 8 Vibration frequency analysis without considering the tool radial runout effect. **a** Stability lobe diagram. **b** Vibration frequency diagram. **c** The relationship between characteristic multiplier and unit circle

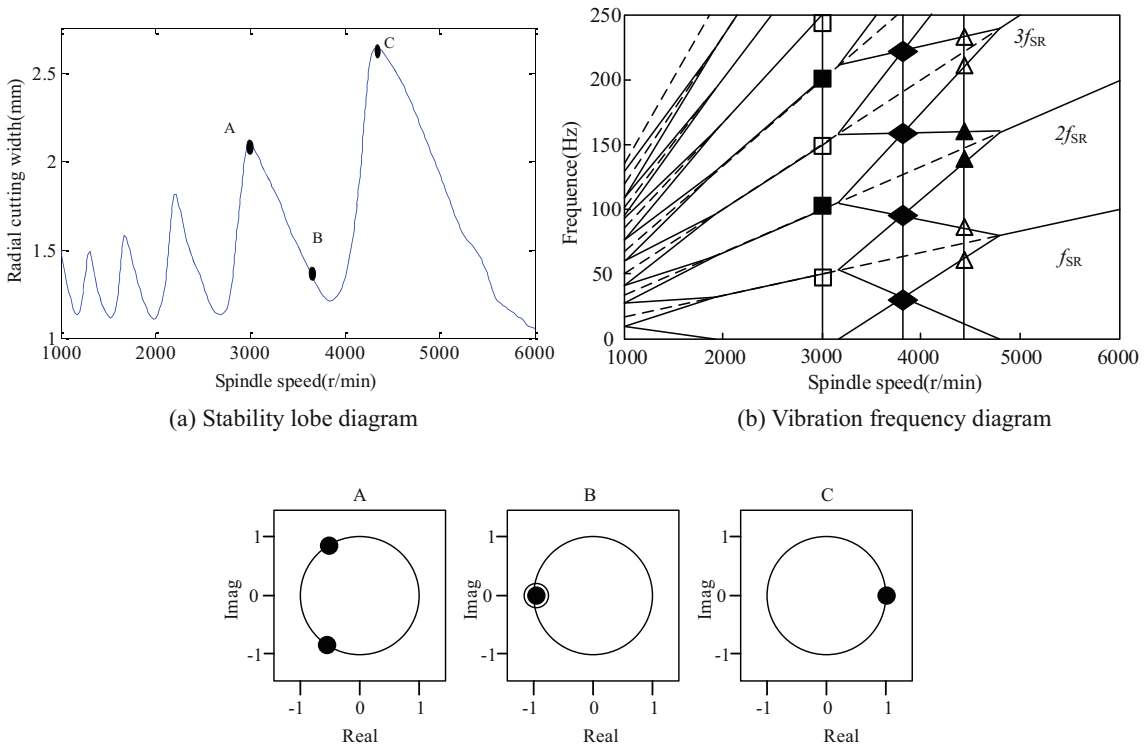

(a) Stability lobe diagram (b) Vibration frequency diagram

(c) The relationship between characteristic multiplier and unit circle

Fig. 9 Vibration frequency analysis without considering the tool radial runout effect. **a** Stability lobe diagram. **b** Vibration frequency diagram. **c** The relationship between characteristic multiplier and unit circle

The stability lobe diagram without considering the tool radial runout effect is higher than that with considering the tool radial runout effect at the spindle speed of 1000~2000 rpm, but the difference is insignificant. The stability lobe diagram with considering the tool radial runout effect is higher than that without considering the tool radial runout effect at the spindle speed of 3000~6000 rpm, the difference increases gradually with the raising of the spindle speed.

In conclusion, the tool radial runout effect can effectively improve the stability of the plunge milling within a certain spindle speed range. The analytical conclusions of this paper are consistent with the results given in Ref. [24–26].

6.3 Vibration frequency analysis

The stability lobe diagram, vibration frequency diagram, and the relationship between characteristic multiplier and unit circle are obtained without considering the tool radial runout effect, as shown in Fig. 8. The tooth passing frequency (f_{TP}) and its higher harmonics are denoted by the dotted line in Fig. 8b. The Hopf bifurcation frequencies for point A are denoted by white squares. The period 2 bifurcation frequencies for point B are denoted by the white triangles. The bifurcation types of point A and point B are confirmed by the relationship between characteristic multiplier and unit circle at point A and point B.

The stability lobe diagram, vibration frequency diagram, and the relationship between characteristic multiplier and unit circle are obtained with considering the tool radial runout effect, as shown in Fig. 9. The spindle rotation frequency (fSP) and its higher harmonics are denoted by the dotted line in Fig. 9b. The Hopf bifurcation frequencies for point A are denoted by white squares. The period 2 bifurcation frequencies for point C are denoted by the white triangles. The period 1 bifurcation frequencies for point B are denoted by the black diamonds. The Hopf bifurcation frequencies caused by the tool radial runout effect are denoted by the black squares. The period 2 bifurcation frequencies caused by the tool radial runout effect are denoted by the black triangles. The bifurcation types of point A, point B, and point C are confirmed by the relationship between characteristic multiplier and unit circle at point A, point B, and point C.

7 Conclusion

A cutting force prediction model considering the tool radial runout effect is established according to the cutter-workpiece contact relationship in plunge milling. The dynamical model with three degrees of freedom is established according to the characteristics of plunge milling and the time-varying delay effect caused by tool radial runout. The stability lobe diagram of the plunge milling process is obtained by the improved semi-discrete method. The simulation results are in good agreement with the experimental results, which verifies the correctness of the model. Meanwhile, the effect of the tool radial runout effect on bifurcation frequency is also studied. The concrete conclusions are as follows.

(1) The maximum error between the experimental cutting force and the simulated cutting force in X, Y, and Z directions is 12.04%, 12.84%, and 13.23%, respectively, which proves the correctness of the cutting force model.
(2) It is found that the maximum difference of cutting forces of different cutting edges on the same cutter in the X, Y, and Z directions caused by the radial runout of the tool is 16%, 18.42%, and 18.18%, respectively.
(3) It can be seen from the range analysis of orthogonal experiment, the radial cutting width is the most important factor affecting the cutting force, followed by the spindle speed and finally the feed per tooth.
(4) The tool radial runout effect can effectively improve the stability of the plunge milling within a certain spindle speed range. The reason is that the tool radial runout effect changes the tool cutting conditions, which in turn interferes with the excitation mechanism of the milling process.
(5) It is found that the tool radial runout effect can produce period 1 bifurcation frequency in the milling non-stationary process, and double the period 2 bifurcation and Hopf bifurcation frequency.

Acknowledgments The authors sincerely thank all the anonymous reviewers for their valuable suggestions on the improvement of our paper.

Funding information This project is supported by Projects of International Cooperation and Exchanges NSFC (51720105009).

References

1. Liu X, Gao H, Yue C, Li R (2018) Investigation of the milling stability based on modified variable cutting force coefficients. Int J Adv Manuf Technol 96(9–12):2991–3002
2. Luo M, Han C (2019) HM Hafeez. Four-axis trochoidal toolpath planning for rough milling of aero-engine blisks. Chin J Aeronaut 32(8):2009–2016
3. Budak E, Altintas Y (1995) Modeling and avoidance of static form errors in peripheral milling of plates. Int J Mach Tool Manu 35(3): 459–476
4. Matsumura T, Usui E (2010) Predictive cutting force model in complex-shaped end milling based on minimum cutting energy. Int J Mach Tool Manu 50(5):458–466
5. Attanasio A, Abeni A, Özel T (2019) Finite element simulation of high speed micro milling in the presence of tool run-out with experimental validations. Int J Adv Manuf Technol 100(1–4):25–35
6. Lee P, Altintaş Y (1996) Prediction of ball-end milling forces from orthogonal cutting data. Int J Mach Tool Manu 36(9):1059–1072

7. Sutherland JW, DeVor RE (1986) An improved method for cutting force and surface error prediction in flexible end milling systems. ASME J Eng Ind 108(4):269–279
8. Wang JJJ, Liang SY (1996) Chip load kinematics in milling with radial cutter runout. J Eng Ind Trans ASME 118(1):111–116
9. Kline WA, DeVor RE (1983) The effect of runout on cutting geometry and forces in end milling. Int J Mach Tool Des Res 23(2–3): 123–140
10. Wang SB, Geng L, Zhang YF (2015) Cutting force prediction for five-axis ball-end milling considering cutter vibrations and run-out. Int J Mech Sci 96:206–215
11. Sun Y, Guo Q (2011) Numerical simulation and prediction of cutting forces in five-axis milling processes with cutter run-out. Int J Mach Tool Manu 51(10–11):806–815
12. Zhu Z, Yan R, Peng F, Duan X, Zhou L (2016) Parametric chip thickness model based cutting forces estimation considering cutter runout of five-axis general end milling. Int J Mach Tool Manu 101: 35–51
13. Zhou L, Peng FY, Yan R, Yao P (2015) Analytical modeling and experimental validation of micro end-milling cutting forces considering edge radius and material strengthening effects. Int J Mach Tool Manu 97:29–41
14. Li K, Zhu K, Mei T (2016) A generic instantaneous undeformed chip thickness model for the cutting force modeling in micromilling. Int J Mach Tool Manu 105:23–31
15. Yue C, Gao H, Liu X, Liang SY (2019) A review of chatter vibration research in milling. Chin J Aeronaut 32(2):215–242
16. Smith S, Tlusty J (1993) Efficient simulation programs for chatter in milling. CIRP Ann 42(1):463–466
17. Altintaş Y, Budak E (1995) Analytical prediction of stability lobes in milling. CIRP Ann 44(1):357–362
18. Merdol SD, Altintas Y (2004) Multi frequency solution of chatter stability for low immersion milling. J Manuf Sci E T ASME 126(3): 459–466
19. Insperger T, Stépán G (2004) Updated semi-discretization method for periodic delay-differential equations with discrete delay. Int J Numer Methods Eng 61(1):117–141
20. Bayly PV, Halley JE, Mann BP (2003) Stability of interrupted cutting by temporal finite element analysis. J Manuf Sci E T ASME 125(2):220–225
21. Ding Y, Zhu LM, Zhang XJ (2010) A full-discretization method for prediction of milling stability. Int J Mach Tool Manu 50(5):502–509
22. Insperger T, Mann BP, Surmann T (2008) On the chatter frequencies of milling processes with runout. Int J Mach Tool Manu 48(10): 1081–1089
23. Wan M, Zhang WH, Dang JW (2010) A unified stability prediction method for milling process with multiple delays. Int J Mach Tool Manu 50(1):29–41
24. Zhang XJ, Xiong CH, Ding Y, Xiong Y (2011) Variable-step integration method for milling chatter stability prediction with multiple delays. Sci China Technol Sci 54(12):3137–3154
25. Zhang X, Zhang J, Pang B, Wu D (2016) An efficient approach for milling dynamics modeling and analysis with varying time delay and cutter runout effect. Int J Adv Manuf Technol 87(9–12):3373–3388
26. Zhang X, Zhang J, Zhang W, Li J (2018) A non-contact calibration method for cutter runout with spindle speed dependent effect and analysis of its influence on milling process. Precis Eng 51:280–290
27. Gao H, Liu X (2019) Stability research considering non-linear change in the machining of titanium thin-walled parts. Materials 12(13):2083
28. Gonzalo O, Beristain J, Jauregi H, Sanz C (2010) A method for the identification of the specific force coefficients for mechanistic milling simulation. Int J Mach Tool Manu 50(9):765–774
29. Yao Q, Luo M, Zhang D, Wu B (2018) Identification of cutting force coefficients in machining process considering cutter vibration. Mech Syst Signal Process 103:39–59
30. Zhai Y, Gao H, Wang Y (2019) Influence of cutting parameters on force coefficients and stability in plunge milling. Int J Adv Manuf Technol:1–11
31. Armarego EJA, Deshpande NP (1991) Computerized end-milling force predictions with cutting models allowing for eccentricity and cutter deflections. CIRP Ann 40(1):25–29
32. Liang SY, Wang JJJ (1994) Milling force convolution modeling for identification of cutter axis offset. Int J Mach Tool Manu 34(8): 1177–1190
33. Wang JJJ, Zheng CM (2003) Identification of cutter offset in end milling without a prior knowledge of cutting coefficients. Int J Mach Tool Manu 43(7):687–697
34. Wan M, Zhang W, Dang J, Yang Y (2009) New procedures for calibration of instantaneous cutting force coefficients and cutter runout parameters in peripheral milling. Int J Mach Tool Manu 49(14):1144–1151